

Spectroscopy of the optical Einstein ring 0047-2808 [★]

S. J. Warren,¹ A. Iovino², P. C. Hewett,³ and P. A. Shaver⁴

¹*Blackett Laboratory, Imperial College of Science Technology and Medicine, Prince Consort Rd, London SW7 2BZ*

²*Osservatorio Astronomico di Brera, Via Brera 28, I-20121 Milano, Italy*

³*Institute of Astronomy, Madingley Road, Cambridge CB3 0HA*

⁴*European Southern Observatory, Karl-Schwarzschild-Strasse 2, D-85748 Garching bei München, Germany*

Received in original form

ABSTRACT

We present optical and near-infrared spectroscopic observations of the optical Einstein ring 0047-2808. We detect both [OIII] lines $\lambda\lambda 4959, 5007$ near $\sim 2.3\mu$, confirming the redshift of the lensed source as $z = 3.595$. The Ly α line is redshifted relative to the [OIII] line by $140 \pm 20 \text{ km s}^{-1}$. Similar velocity shifts have been seen in nearby starburst galaxies. The [OIII] line is very narrow, 130 km s^{-1} FWHM. If the ring is the image of the centre of a galaxy the one-dimensional stellar velocity dispersion $\sigma = 55 \text{ km s}^{-1}$ is considerably smaller than the value predicted by Baugh et al. (1998) for the somewhat brighter Lyman-break galaxies. The Ly α line is significantly broader than the [OIII] line, probably due to resonant scattering. The stellar central velocity dispersion of the early-type deflector galaxy at $z = 0.485$ is $250 \pm 30 \text{ km s}^{-1}$. This value is in good agreement both with the value predicted from the radius of the Einstein ring (and a singular isothermal sphere model for the deflector), and the value estimated from the $D_n - \sigma$ relation.

Key words: gravitational lensing – galaxies: formation

1 INTRODUCTION

Warren et al. (1996a, hereafter Paper I) reported observations of the first candidate Einstein ring to be discovered at optical wavelengths. Confirmation that the system is a gravitational lens, via the detection of a second emission line which secured the source redshift, was recorded as a note added in proof. Here we present the confirmatory spectrum together with additional optical and near-ir spectra of the source and deflector galaxies. The lens system, designated 0047-2808, is the first example of a normal galaxy lensing another normal galaxy, albeit one at high-redshift and probably representing an early phase in the evolution of normal galaxies. The deflector is a massive early-type galaxy, redshift $z = 0.485$, and the source a star-forming object at redshift $z = 3.595$. Resolved observations of the extended surface brightness distribution around the ring using the Hubble Space Telescope offer the prospect of providing powerful constraints on models of the deflector and the source in a fashion similar to that achieved with Einstein rings discovered at radio wavelengths (Kochanek 1995).

The detection of 0047-2808 highlights a number of important advantages of the survey technique (Warren et al. 1996b) employed in the system's identification. The deflector population, luminous early-type galaxies with redshifts $0.3 \leq z \leq 0.5$, is homogeneous and well-defined, and the deflector redshift is readily obtained. The source population, optically faint high-redshift star-forming systems that exhibit emission lines, notably Ly α $\lambda 1216$, is of particular interest in charting the history of star-formation associated with the population of normal galaxies, and, as with the deflectors, the object redshift is readily obtained. The acquisition of redshifts for deflector and source means that the lensing geometry is fully defined and contrasts with the difficulties experienced in establishing the redshifts of source and deflector in lenses discovered at radio wavelengths (see summary by Keeton and Kochanek 1996).

In Section 2 new optical spectroscopic observations are described, and the procedure used to measure the velocity-dispersion of the deflector galaxy detailed. Infrared spectroscopy of the restframe wavelength region including the [OIII] $\lambda\lambda 4959, 5007$ emission lines is presented in Section 3. Section 4 contains a discussion of the implications of the results for the nature of the source and deflector galaxies.

[★] Based on observations obtained at the European Southern Observatory, La Silla, Chile, and the United Kingdom Infrared Telescope, Hawaii.

2 OPTICAL SPECTROSCOPY

2.1 Observations

Optical spectra of 0047-2808 were obtained at the ESO NTT equipped with the EMMI instrument in spectroscopic mode, on 1995 October 1 UT. Atmospheric conditions were not ideal with the seeing averaging $1''.2$ and a strong wind throughout the night. A 6001/mm grating blazed at 6000\AA was employed in the EMMI red arm, with a Tektronix 2048×2048 CCD as the detector. The CCD was binned by a factor of two in the dispersion direction, giving a pixel size of $0''.27 \times 1.3\text{\AA}$, and a wavelength coverage of $5400 - 6700\text{\AA}$. The slit was oriented at $\text{PA} = 45^\circ$ to include the bright part of the lensed ring.

Four 2400 s exposures of the 0047-2808 system were made through a $1''.5$ slit. The resulting spectra have a resolution of $\sim 3.25\text{\AA}$ and include the $\text{Ly}\alpha$ $\lambda 1216$ emission line of the source galaxy at 5589\AA , and the 4300\AA G-band absorption feature in the deflecting galaxy at $\sim 6390\text{\AA}$.

The EMMI blue arm was used with a slit width of $0''.75$ to obtain spectra centered on the G-band absorption feature of three stars to act as velocity-dispersion templates. The stars, HD8779, HD203638, and HD223311, are of spectral type K0III, K0IV, and K4III respectively. The resulting spectra have a resolution of $\sim 1.13\text{\AA}$ and a wavelength coverage that exceeded that of the equivalent rest-frame region accessible in the observations of the lensing galaxy.

2.2 Spectroscopic reductions

Data reduction employed standard routines available in IRAF[†] for bias, dark, and flat field correction, and the removal of cosmic rays. Variance-weighted one dimensional spectra were extracted using an aperture width of 16 pixels, $4''.3$. The spectra were rebinned to a linear vacuum wavelength scale using 1.3\AA and 0.45\AA pixels for the red and blue arms respectively. The rms residuals for individual calibration lines about the adopted wavelength solution were 0.13\AA and 0.02\AA respectively.

The galaxy spectra were calibrated onto a relative flux scale using spectra taken of a flux standard. The four galaxy spectra were then coadded using variance weighting to produce a combined spectrum, shown in Figure 1. The zero-point of the flux scale was determined by equating the flux in the spectrum integrated over a broad V filter band-pass with the V total magnitude of the galaxy measured in the direct CCD image of Paper I. The signal-to-noise ratio over the wavelength range $6100 - 6700\text{\AA}$ in the final coadded galaxy spectrum was $\sim 7 \text{ pix}^{-1}$. The signal-to-noise ratios over the wavelength range $4100 - 4500\text{\AA}$ in the three stellar template spectra were ~ 400 (HD8779), ~ 100 (HD203638), and ~ 250 (HD223311).

[†] IRAF is distributed by the National Optical Astronomy Observatories, which are operated by the Association of Universities for Research in Astronomy, Inc. under contract with the National Science Foundation

2.3 Source emission line properties

In order to measure the central wavelength and full width half maximum (FWHM) of the $\text{Ly}\alpha$ $\lambda 1216$ emission line we first subtracted a redshifted and scaled template spectrum of an elliptical galaxy. A low-order polynomial was then fitted to regions on either side of the line in order to remove any residuals and a Gaussian profile was then fitted, weighted by the errors as a function of wavelength. The central wavelength was then corrected to the heliocentric value. The results are listed in Table 3. The values are in good agreement with those listed in Paper I, measured from a lower resolution and lower signal-to-noise ratio spectrum.

2.4 Deflector velocity dispersion

The Fourier cross-correlation technique of Tonry and Davis (1979) was employed to determine the velocity dispersion of the lensing galaxy, restricting the wavelength coverage to the restframe region $4100 - 4500\text{\AA}$. Measurements using the FXCOR task within the IRAF package RV were calibrated using the procedure described by Falco et al. (1997) to which the reader is referred for further details. In outline, a cross-correlation between the galaxy and stellar-template spectra is performed after first smoothing the template spectra to the same resolution as the galaxy spectrum (FWHM $\sim 160 \text{ km s}^{-1}$ at $\sim 4300\text{\AA}$ restframe in our case). A Gaussian is then fit to the central portion of the resulting cross-correlation peak to give a measure of the FWHM. The galaxy velocity dispersion is estimated via a calibration curve relating input velocity dispersion to measured FWHM. The calibration curve is created by convolving each stellar template with a series of Gaussians of different width, and cross correlating against the original template. For the continuum subtraction, apodizing, and filtering we followed closely the recommendations of Tonry and Davis (1979).

Table 1 lists, for each template spectrum, the measured FWHM of the cross-correlation peak, the inferred σ_v from the associated calibration curve, and the R-value, a measure of the signal-to-noise ratio of the correlation peak (Tonry and Davis 1979).

The template that most closely matches the galaxy spectrum in the strength of the absorption features is HD8779, spectral type K0III, while HD223311, with the rather late spectral type of K4III, gives the lowest value for σ_v . Assigning equal weight to the value obtained using each template and taking the standard error among the three measurements leads to an estimate of $249 \pm 10 \text{ km s}^{-1}$. However, the signal-to-noise ratio of the galaxy spectrum is low and varying the parameters that control the filtering of the Fourier components produces differences of $\lesssim 20 \text{ km s}^{-1}$. Varying the range over which the Gaussian fit to the cross-correlation is performed by $\pm 10\%$ also produces differences of $\lesssim 20 \text{ km s}^{-1}$. Therefore we adopt $250 \pm 30 \text{ km s}^{-1}$ as the estimate of the galaxy velocity dispersion.

3 NEAR-INFRARED SPECTROSCOPY

3.1 Observations

Spectra in the K window covering the wavelengths of redshifted $\text{H}\beta$ $\lambda 4861$ and $[\text{OIII}]$ $\lambda\lambda 4959, 5007$ in the lensed

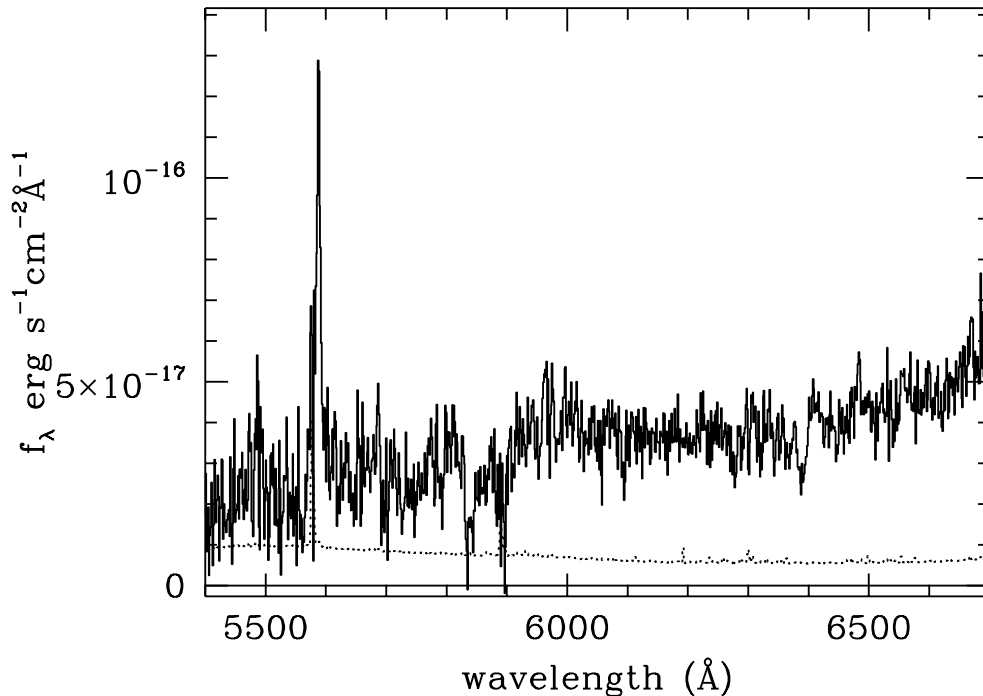


Figure 1. Combined optical spectrum showing the G band (near 6400Å) and H+K (near 5900Å) absorption lines in the deflector galaxy, and the Ly α emission line (at 5589Å) from the source galaxy. The dotted line shows the 1σ error for each pixel. The pixel size is 1.31 Å. The spectrum has been scaled to the correct total magnitude.

Table 1. Velocity dispersion estimates

Template	FWHM km s ⁻¹	σ_v km s ⁻¹	R-value
HD8779	578	250	5.8
HD203638	600	260	5.8
HD223311	582	237	5.9

source were obtained in 1995, 1996, and 1997 using the CGS4 instrument on the United Kingdom Infrared Telescope. The journal of observations appears in Table 2. As with the optical observations the slit was aligned in a manner so as to cover the region of emission where the ring is bright. For the 1995 and 1996 observations the slit was centered on the galaxy oriented at the position angles (PAs) listed in Table 2 i.e. pointing at the region where the ring is bright. For the 1997 observations the slit was instead centered on the region where the ring is bright and aligned tangentially to the ring.

The observing procedure involved nodding the galaxy between two positions on the slit. If necessary, as indicated in Table 2, at each nod position the spectrum was sub-stepped by 0.5 pixel in the wavelength direction to recover the full sampling of the undersampled spectra by interleaving exposures.

3.2 Spectroscopic reductions

The data reduction mostly followed the standard CGS4 methodology for combining all the frames, with the excep-

tion of the use of a sigma-clipping algorithm in summing the sets of co-added integrations at each nod position (in order to improve the rejection of cosmic rays), and an improved polynomial fit for second-order sky subtraction. For the 1996 observations the failure of the CGS4 slit rotation mechanism resulted in sky lines that were tilted away from the perpendicular to the dispersion direction and it was necessary to apply a distortion correction to straighten the frames.

A variance frame was created by measuring the variance in the counts in each column, excluding the pixels containing the object spectrum, and assuming this single value was applicable to each pixel within the column. This estimate agreed well with the variance computed assuming Poisson statistics. One-dimensional spectra were then extracted from the data and variance frames, using apertures 1.2 arcsec wide for spectra A, B, C, and 1.8 arcsec wide for spectrum D. The spectra from the two nod positions were combined and the resulting spectrum rebinned onto a linear vacuum wavelength scale. Finally the spectra were flux calibrated using observations of standard stars.

3.3 Source emission line properties

The four K-band spectra are useful in a variety of ways. Because of the wide slit used, the spectra A and B will provide reasonably accurate measures of line fluxes (provided the surface brightness profile around the ring in the light of [OIII] is similar to that in Ly α). Therefore spectra C and

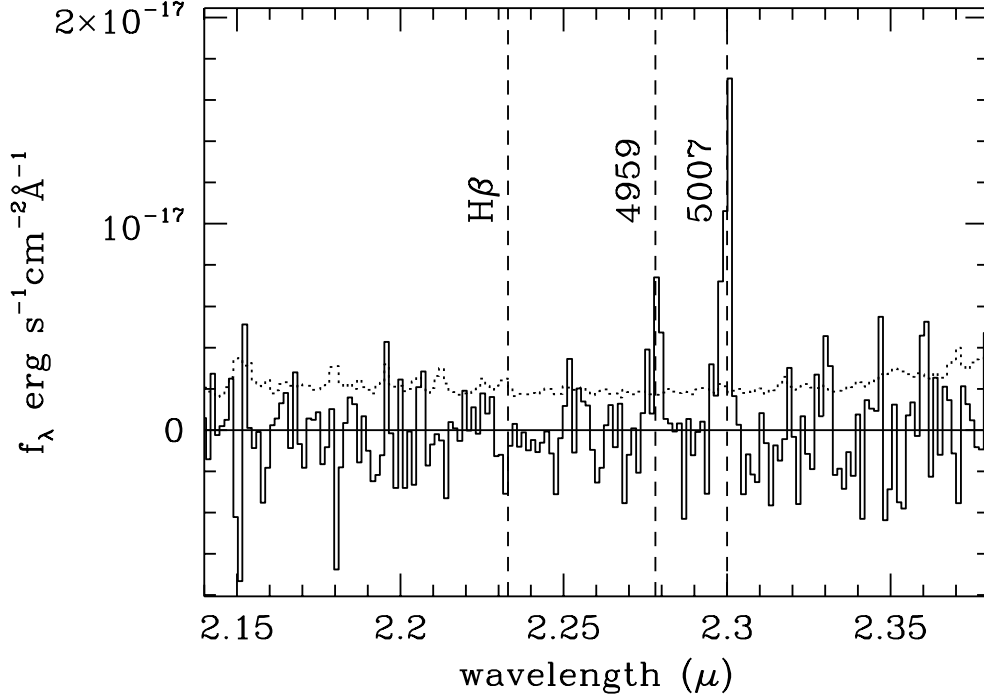


Figure 2. Combined near-infrared spectrum showing the detected [OIII] $\lambda\lambda$ 4959 and 5007 lines. This spectrum is an optimal combination of the 4 spectra A, B, C, D, after subtraction of the continuum. The spectra were rebinned to the largest pixel size of the 4 spectra $0.0014\mu\text{pix}^{-1}$ wide. The dotted line shows the 1σ error for each pixel. The position of $H\beta$ is marked but the summed flux at this wavelength is negative.

Table 2. Journal of near-infrared spectroscopy

UT date	spectrum	slit width arcsec	grating l mm^{-1}	order	sub-step	resolving power	position angle	integration time sec
1995 Oct 1	A	2.4	75	1	2	450	45	3520
1996 Jul 31	B	2.4	150	1	1	900	45	1920
1996 Aug 1, 2	C	1.2	150	1	2	1640	45, 0	2520
1997 Dec 6	D	1.2	150	2	1	3560	-45	3840

D, taken with a narrower slit, were scaled to the correct total flux using the measured flux in the [OIII] 5007 line. In each spectrum a low-order polynomial fit was used to subtract the continuum, and the four spectra were then averaged with weightings proportional to the inverse variance. The final combined spectrum is plotted in Fig. 2.

Table 3 lists the measured flux in the [OIII] 5007 line. Also provided is the 3σ upper limit to the flux in the $H\beta$ line. The summed flux over 5 pixels at the position of $H\beta$ is negative. The flux limit quoted is simply three times the 1σ error on the summed flux at that wavelength i.e. we ignored that the measured flux is negative. The central wavelength of the [OIII] 5007 line was measured from spectra C and D, and corrected to the heliocentric value. Spectra A and B are not useful for this measurement because the large width of the slit means that the surface brightness of the source galaxy may be non-uniform across the slit so that the centroid of the flux may not coincide with the centre of the slit. Finally the width of the [OIII] line was measured from spectrum D.

The line is unresolved in the other three spectra. The line width was measured by simultaneously fitting Gaussians, of line-flux ratio 3:1, to the redshifted 5007 and 4959 lines. The value quoted in Table 3 is the intrinsic width i.e. after quadrature subtraction of the instrument profile. A plot of the velocity profile of the [OIII] 5007 line in spectrum D is provided in Fig. 3. In the following section we compare the redshift and line width of the [OIII] line measured from spectrum D with the corresponding values for $\text{Ly}\alpha$. This assumes that we have sampled the same part of the ring for both spectra. This is close to the truth, since both spectra were centered on the SW quadrant of the ring. For the $\text{Ly}\alpha$ line a section of the ring 1.5 arcsec long (the slit width) is represented in the spectrum. For the [OIII] line, with the slit in a perpendicular orientation, a section 1.8 arcsec long (the extraction aperture) was sampled.

4 DISCUSSION

Table 3. Properties of the Ly α , H β , and [OIII] 5007 lines

	Ly α	H β	[OIII] 5007
^a Central wavelength λ	$5589.1 \pm 0.2 \text{ \AA}$		$2.3008 \pm 0.0001 \mu$
^a Redshift	3.5974 ± 0.0002		3.5953 ± 0.0002
^b Intrinsic FWHM km s ⁻¹	390_{-75}^{+50}		130_{-60}^{+40}
^c Line flux erg s ⁻¹ cm ⁻²	$(6.0 \pm 0.6) \times 10^{-16}$	$< 2.0 \times 10^{-16} (3\sigma)$	$(6.0 \pm 0.8) \times 10^{-16}$

^a vacuum heliocentric value

^b FWHM errors are 2σ , but 1σ for other parameters

^c Ly α flux from narrow-band image (Paper I)

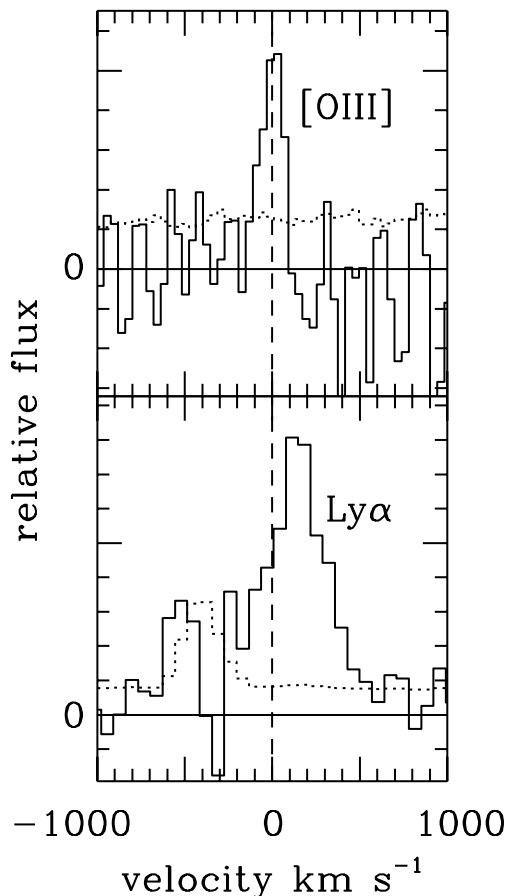


Figure 3. Comparison of the redshift and width of the [OIII] 5007 (spectrum D) line and the Ly α line. The solid lines show the continuum-subtracted spectra, and the dotted lines the 1σ error spectra. Notice that the Ly α line is redshifted relative to the [OIII] line and is also broader.

4.1 The source galaxy

4.1.1 Redshift of the source galaxy

The primary result of the near-ir spectroscopy of the source galaxy is the detection of two emission lines near 2.3μ (Fig. 2). The lines are redshifted [OIII] $\lambda\lambda$ 4959 and 5007 match-

ing with Ly α 1216 in the optical at 5589\AA . This establishes the redshift of the source as $z = 3.595$ and confirms this system as a gravitational lens.

In Fig 3 the velocity profiles of the [OIII] 5007 and Ly α lines are compared. The velocity zero point for both plots is the redshift measured from the [OIII] 5007 line. Two differences between the lines are apparent. Firstly the Ly α line is substantially broader than the [OIII] line and is considered further below. Secondly it is noticeable that the Ly α line is redshifted relative to the [OIII] line. The velocity difference is $140 \pm 20 \text{ km s}^{-1}$. This probably has two causes. Firstly a redward shift of the centroid of the Ly α line has also been seen in those nearby starburst galaxies which display Ly α emission (e.g. Lequeux et al 1995) and this is related to the kinematics of the gas in the starburst galaxy and to the escape path of the resonantly-scattered Ly α photons. This mechanism may therefore be partly responsible for the velocity shift seen in Fig. 3. In addition absorption of the blue wing of the Ly α emission line by intervening cosmologically-distributed Ly α -forest clouds may contribute to the redward shift of the line centroid. If so the intrinsic width of the Ly α line is even larger than the value quoted in Table 3.

4.1.2 Velocity dispersion of the source galaxy

The second important result of the near-ir spectroscopy is the measurement of the width of the [OIII] $\lambda\lambda$ 4959, 5007 lines. The intrinsic width of the [OIII] line (Table 3) is 130 km s^{-1} FWHM. This corresponds to a one-dimensional velocity dispersion of only $\sigma = 55 \text{ km s}^{-1}$. Such a low value could be explained if, for example, we are imaging a region of star formation in a disk, away from the nucleus. On the other hand the high-redshift galaxies discovered by Steidel et al (1996) are very compact so it is quite likely that the ring is the image of the centre of a galaxy. In this case the galaxy mass is very small compared to the mass of typical galaxies today. This result accords in a general way with the hierarchical picture of galaxy formation in which today's galaxies were in several pieces at $z > 3$. However the measured velocity dispersion then appears low in comparison with the results of the calculations of Baugh et al (1998) who used a semi-analytic approach to predict the velocity dispersion of the Lyman-break galaxies discovered by Steidel et al (1996). Although the magnitude range they considered ($\mathcal{R}_{AB} < 25$) is somewhat brighter than the unlensed magnitude of the source galaxy, $V \sim 27$ (Paper I), the predicted velocity dis-

persions $> 200 \text{ km s}^{-1}$ are several times larger than the value measured for the ring.

Clearly it is of interest to detect other lensed systems similar to 0047-2808 in order to measure the distribution of line widths. The advantage of lensed systems is the flux amplification (~ 20 for 0047–2808) enabling higher S/N measurements and the possibility of observing fainter sources. These results will complement the work of Pettini et al (1998) who have begun a programme of K-band measurements of the line widths of the brightest Lyman-break galaxies.

4.1.3 Dust in the source galaxy

The width of the Ly α emission line $390_{-75}^{+50} \text{ km s}^{-1}$ FWHM (2σ limits) is significantly greater than the width of the [OIII] line $130_{-60}^{+40} \text{ km s}^{-1}$ FWHM. This is probably due to resonant scattering of the Ly α photons which diffuse in frequency over the multiple scatterings during their escape through a cloud of neutral hydrogen.

Because the escape path length of the Ly α photons is much greater than for the continuum photons, the line is extinguished selectively relative to the continuum. We now show how it is possible to combine the measured width and flux of the Ly α line with the flux of one of the Balmer lines to estimate the dust-to-gas ratio in the gas cloud. Consider a source of Ly α photons escaping from the mid-plane of a plane-parallel slab of neutral hydrogen. The line width is a measure of the face-on column density of the cloud, because the broadening of the emerging Ly α line is a function of the number of times the escaping photons are scattered. The line width is proportional to the cube root of the column density (e.g. Adams 1972). The extinction is also related to the number of times the photons are scattered, and to the dust-to-gas ratio. Therefore the extinction of the line is related to the line width Δv and the dust-to-gas ratio. Since the extinction can be measured by comparing the strength of the Ly α line to one of the Balmer lines, the measurement of the Ly α line width yields a measurement of the dust-to-gas ratio.

In detail, Warren and Møller (1996) provided the following expression for the fraction of escaping Ly α photons:

$$f_e = \text{sech}[(\Delta v/147)^2(\sigma/10)^{-1}(k\delta/0.2)^{1/2}0.143] \quad (1)$$

where $k \equiv 10^{21}(\tau_B/N_{H1}) \text{ cm}^{-2}$ is the dimensionless dust-to-gas ratio, δ is the ratio of the absorption optical depth in the continuum near Ly α to that in the B band τ_B (Charlot and Fall 1991), and σ is the velocity dispersion of the neutral gas, taken here to be 10 km s^{-1} . The Case B ratio of the Ly α and H β line fluxes is ~ 25 , while the measured ratio is > 3 (Table 3). Therefore the Ly α line has been extinguished by a factor $1/f_e$ no more than 8. Inserting this limit into the above equation we obtain a limit to the dust-to-gas ratio $k\delta < 1.5$.

This limit is not particularly stringent. For example Fall, Pei, and McMahon (1989) obtained a measurement of $k\delta \sim 0.2$ in high-redshift damped Ly α clouds, from the reddening of the background quasars. Nevertheless the method is an independent one and the limit could be made lower by obtaining a deeper spectrum at H β . For a lower-redshift galaxy the stronger H α line could be used. In a galaxy where both H α and H β could be measured the Balmer decrement

would provide a consistency check since the line ratio can be predicted knowing both the inferred column density and the dust-to-gas ratio.

4.2 Velocity dispersion of the deflector galaxy

In Paper I we estimated the value of the stellar central velocity dispersion σ_c of the lensing galaxy by two methods based on the measured galaxy surface-brightness profile. The Faber-Jackson and $D_n - \sigma$ relations yielded values of $\sigma_c = 280(260) \pm 50 \text{ km s}^{-1}$, and $\sigma_c = 300(265) \pm 35 \text{ km s}^{-1}$ respectively, for $q_0 = 0.1$ (0.5). The measured value of $\sigma_c = 250 \pm 30 \text{ km s}^{-1}$, reported above, is consistent with both estimates. In Paper I we also computed the lens velocity dispersion using the angular size of the ring, and the singular isothermal sphere as a model for the mass profile of the galaxy. This provides an estimate of the velocity dispersion of the dark matter σ_{DM} . The lens angular radius of 1.35 arcsec implies a value $\sigma_{DM} = 270(265) \text{ km s}^{-1}$. The measured value of σ_c is also consistent with this estimated value of σ_{DM} . This result bears on the question of the expected value of the ratio of σ_{DM}/σ_c . Kochanek (1993) argued that the ratio will be close to one, rather than the value $\sqrt{3/2}$ adopted by Turner, Ostriker, and Gott (1984). This difference is important in making predictions of the expected number of lenses, and their angular separations, using measured values of σ_c for nearby galaxies. As compared with the lower value, adoption of the larger value leads to predictions of over twice as many lenses, with separations 50% larger (Kochanek 1993). The measured ratio $\sigma_{DM}/\sigma_c = 1.08(1.06) \pm 0.13$, for $q_0 = 0.1$ (0.5), is consistent with both values. It is feasible with an 8m-class telescope to measure σ_c with sufficient accuracy to provide unambiguous discrimination between the alternatives. Indeed it would be possible to measure the velocity dispersion profile, which, combined with a deep high-resolution image of the ring, could be used to test detailed models of the stellar dynamics and mass distribution in the deflector galaxy.

Acknowledgments

We are particular grateful to J. Davies, T. Geballe, S. Leggett, and S. Ramsay Howat who undertook the various UKIRT CGS4 observations on our behalf as part of the UKIRT service programme. The authors acknowledge the data analysis facilities provided by the Starlink Project which is run by CCLRC on behalf of PPARC.

REFERENCES

- Adams T. F., 1972, ApJ, 174, 439
- Baugh C.M., Cole S., Frenk C.S., Lacey C.G., 1998, ApJ, in press (astro-ph/9703111)
- Charlot S., Fall S. M., 1993, ApJ, 378, 471
- Falco E.E., Shapiro I.I., Moustakas L.A., Davis M., 1997, ApJ, 484, 70
- Fall S.M., Pei Y.C., McMahon R.G., 1989, ApJ, 341, L5
- Keeton C., Kochanek C.S., 1996, in *Astrophysical Applications of Gravitational Lensing*, edited by C.S. Kochanek and J.N. Hewitt, (Kluwer, Dordrecht), p. 419
- Kochanek C.S., 1993, ApJ, 419, 12
- Kochanek C.S., 1995, ApJ, 445, 559

- Lequeux J., Kunth D., Mas-Hesse J.M., Sargent W.L.W., 1995, A&A, 301, 18
- Pettini M., Kellogg M., Steidel C.C., Dickinson M., Adelberger K.L., Giavalisco M., 1998, ApJ, submitted.
- Steidel C.C., Giavalisco M., Pettini M., Dickinson M., Adelberger K.L., 1996, ApJ, 462, L17
- Tonry J., Davis M., 1979, AJ, 84, 1511
- Turner E.L., Ostriker J.P., Gott J.R., 1984, ApJ, 284, 1
- Warren S.J., Møller P., 1996, A&A ,311, 25
- Warren S.J., Hewett P.C., Lewis G.F., Møller P., Iovino A., Shaver P.A., 1996a, MNRAS, 278, 139 (Paper I)
- Warren S.J., Hewett P.C., Lewis G.F., Møller P., Iovino A., Shaver P.A., 1996b, in *Astrophysical Applications of Gravitational Lensing*, edited by C.S. Kochanek and J.N. Hewitt, (Kluwer, Dordrecht), p. 329

This paper has been produced using the Royal Astronomical Society/Blackwell Science L^AT_EX style file.